energies

MDPI

Article

Experimental Study of Evaporation Characteristics of Acoustically Levitated Fuel Droplets at High Temperatures

Bin Pang [1,2,*], Guangcan Yang [3], Xiaoxin Liu [1,2,*], Yu Huang [3], Wanli Li [1,2], Yongqing He [3], Zhongyuan Shi [3], Zhaochu Yang [3,*] and Tao Dong [4]

1 State Key Laboratory of Engine and Powertrain System, Weifang 261061, China
2 Engine Research Institute, Weichai Power Co., Ltd., Weifang 261061, China
3 Chongqing Key Laboratory of Micro-Nano Systems and Intelligent Transduction, Chongqing Technology and Business University, Chongqing 400067, China
4 Department of Microsystems, Faculty of Natural Sciences, Technologies, and Marine Studies, University of South-Eastern Norway, 3184 Horten, Norway
* Correspondence: pangb@weichai.com (B.P.); liuxiaox@weichai.com (X.L.); zhaochu.yang@ctbu.edu.cn (Z.Y.)

Abstract: Examining fuel droplet evaporation is crucial for enhancing fuel engine efficiency, conserving energy, and reducing emissions. This study utilizes experimental methods involving ultrasonic standing wave levitation and high-speed cameras to investigate the impact of temperatures and droplet properties, including initial diameter and composition, on the evaporation process. The evaporation behaviors of fuel droplets, like hexadecane and diesel, are documented across a temperature spectrum spanning 150 °C to 550 °C, with an initial droplet equivalent diameter ranging from 0.10 to 0.30 mm. The evaporation rate positively correlates with temperature and may vary by 15% to 71% between hexadecane and diesel droplets.

Keywords: fuel droplet evaporation; high temperature; acoustical levitation; initial diameter

Citation: Pang, B.; Yang, G.; Liu, X.; Huang, Y.; Li, W.; He, Y.; Shi, Z.; Yang, Z.; Dong, T. Experimental Study of Evaporation Characteristics of Acoustically Levitated Fuel Droplets at High Temperatures. *Energies* **2024**, *17*, 271. https://doi.org/10.3390/en17010271

Academic Editor: Leszek Chybowski

Received: 13 November 2023
Revised: 22 December 2023
Accepted: 27 December 2023
Published: 4 January 2024

1. Introduction

Fuel droplet atomization, evaporation, and combustion are crucial for enhancing fuel efficiency and mitigating emissions for a direct-injection, internal combustion engine that utilizes liquid fuel [1–4]. The evaporation of fuel droplets within the cylinder during the operational cycle is a significant factor in creating the combustible gas mixture. Consequently, scientists have been undertaking efforts to comprehend the mechanism of fuel droplet evaporation [5,6].

Acoustic levitation works for spray polymerization and particle morphology in a model system. The non-contact nature of acoustic levitation avoids specimen–receptacle touch, which is an advantage [7]. The heat and mass transmission properties of fuel droplets may be studied experimentally using this method [8–11]. Due to the prevailing global trend towards energy preservation and emission reduction, it is inevitable that alterations to the environmental conditions within the cylinder of an industrial engine will impact the fuel evaporation and oil–gas mixing processes. Consequently, acoustically levitated droplet evaporation has been investigated for decades [12–14]. However, the details of the evaporation mechanism of fuel droplets in a supercritical environment still need to be better understood [15–17].

Fuel droplet evaporation is a complex process that includes several variables. We have to learn more about droplet evaporation theory because of the tests under various conditions. Therefore, it is of utmost importance to conduct experimental research on the suspension of fuel droplets at a particular temperature, observe and record droplet evaporation, and conduct quantitative analysis on the heat and mass transfer model. In this experimental investigation with a high-speed camera, we record the images of transient droplet evaporation and examine the effects of temperature, droplets' physical

and chemical characteristics, their starting diameter, and sonic levitation on the evaporation characteristics of fuel droplets, including hexadecane and diesel.

2. Acoustically Levitated Droplet

Various factors, including resistance, inertia, gravity, and acoustic radiation, can affect a droplet moving through a standing acoustic wave field. This secondary, time-independent flow is caused by the levitated droplet's role as a barrier to the periodic acoustic boundary-layer flow [18]. The flow, which comprises an inner and exterior flow, can be manipulated [19]. Evaporation, concentration distribution, and droplet surface temperature distribution may affect fluid-type-dependent flow structure [20–24].

The behavior of the droplet surface is primarily influenced by two key factors: the surface tension force and the acoustic radiation force [25–27], denoted as F_a, which work together to maintain the droplet in suspension (refer to Figure 1).

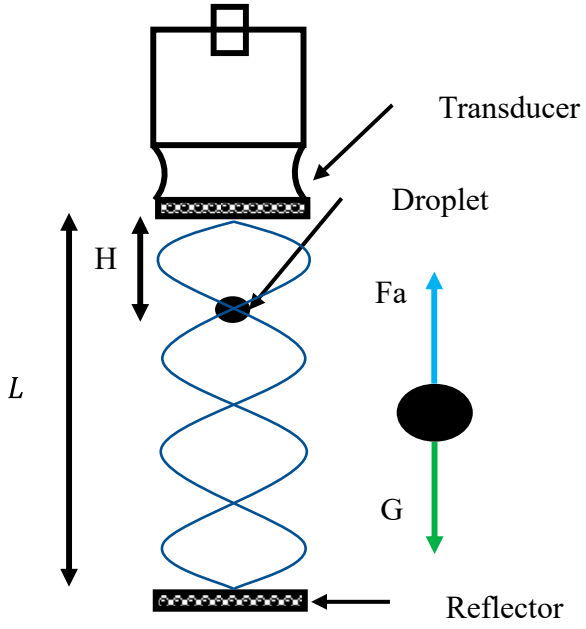

Figure 1. Physical model of an acoustically levitated droplet.

The ultrasonic wavelength:

$$\lambda = \frac{c_0}{f} \tag{1}$$

where c_0 represents the velocity of sound propagation and f represents the frequency.

The acoustic radiation force:

$$F_a = \frac{5}{48}\rho_g n A^2 D^3 sin(2nH) \tag{2}$$

where A denotes the incident amplitude, n represents the number of ultrasounds, $n = 2\pi/\lambda$, ρ_g is the media density, D is the droplet diameter, and H denotes the vertical distance between the center of the droplet and the transducer.

Acoustic suspension is affected by temperature, which shows that the medium density (Equation (3)) and sound velocity (Equation (4)) change with temperature.

$$\rho_g = \rho_0 \frac{273}{T} \tag{3}$$

$$c_0 = 331.6 + 0.6(T - 273.15) \tag{4}$$

where ρ_0 represents the density of the gas at standard atmospheric pressure and T = 273.15 K, and T is the absolute temperature of the surrounding gas, $T = °C + 273.15$.

The droplet gravity:

$$G = \frac{1}{6}\pi D^3 \rho_l g \tag{5}$$

where ρ_l is the droplet density and g is the gravity level.

3. Experimental Methodology

The setup of an experimental system for suspending ultrasonic standing waves at high temperatures is illustrated in Figure 2. The details of the acoustic levitation system are described in our previous work [28]. The system comprises critical components, including an ultrasonic standing wave generator with a frequency of 21.5 ± 0.8 kHz, a droplet transport device, and a heating cylinder.

The ultrasonic standing wave generator has a frequency f = 21.5 ± 0.8 kHz and an output amplitude 50~80 μm, which can work in the temperature range of 0~750 °C. The distance between the transmitting end and the reflecting end is set to L = 40 mm, which can generate n = 5 standing wave nodes. The suspension reflector is equipped with a micro-lifting platform to adjust the ultrasonic suspension of droplets at the order of 20 μm.

The droplet transport device includes an L-shaped quartz tube, a capillary tube, a water bath cycle, and a stepper motor. The droplets in the experiment were produced using a microliter syringe. The inner diameter of the pinhole is 0.2 mm, and the droplet generated in the ultrasonic standing wave field is usually between 0.1 and 1 mm. The drop volume can be selected with an uncertainty of ±0.05 μL. In general, an experiment begins with a drop volume 10% larger than the nominal volume, and then the droplet volume decreases during evaporation. From there, the data regarding the required volume are recorded.

To measure the transient evaporation characteristics of liquid droplets at a high-temperature condition, the high-speed camera pco.dimax is connected to the software pco.camware64, with a frame rate of 1000~2000 FPS. The experimental electric furnace is used to heat up the cylinder, with a PID automatic control LED digital display. Additionally, a thermocouple sensor is used to measure the local temperature in the cylinder; a temperature controller is used to maintain the expected temperature with an accuracy $\leq \pm 5$ °C.

The droplet levitated in the acoustic field has been observed as an ellipsoid [29]. And, as evaporation proceeds, the droplets tend to be spherical. The aspect ratio, $AR = b/a$, can be used to characterize the droplet shape [12]. The diameter of the droplet should be determined through the calculation $D = \sqrt[3]{ba^2}$, where D denotes the equivalent diameter, a denotes the primary diameter, and b means the semi-diameter [30] (Figure 2a). It is important to highlight that the method remains effective even when the droplet is spherical in shape. The droplet diameter presented by the binary image was determined through the ellipse fitting process using Python 3 programming and OpenCV library (Figure 2b). As the initial droplet observed in this experiment is obtained by breaking a large droplet through ultrasonic radiation force, the volume of the initial droplet cannot be estimated. Nevertheless, the approach mentioned above has been proven to exhibit high precision, with a presentation accuracy of approximately 2.5% in droplet volume [31].

Variations in the liquid's surface are indicative of its evaporation behaviors [32],

$$K_\eta = \frac{D_0^2 - D_\eta^2}{t_\eta} \tag{6}$$

where D_0 denotes the initial diameter and D_η and K_η, respectively, denote the instant diameter and the instant evaporation rate at the time t_η.

The mean evaporation rate, which is calculated according to the evaporation rate of a suspension droplet at the steady-state evaporation stage, is taken as the droplet evaporation rate, K, which is calculated by

$$K = \frac{1}{N} \sum_{\eta=t_1}^{\eta=t_N} K_\eta \tag{7}$$

where t_1 is a time point to enter the steady-state evaporation stage and t_N is the point at which droplet evaporation ends.

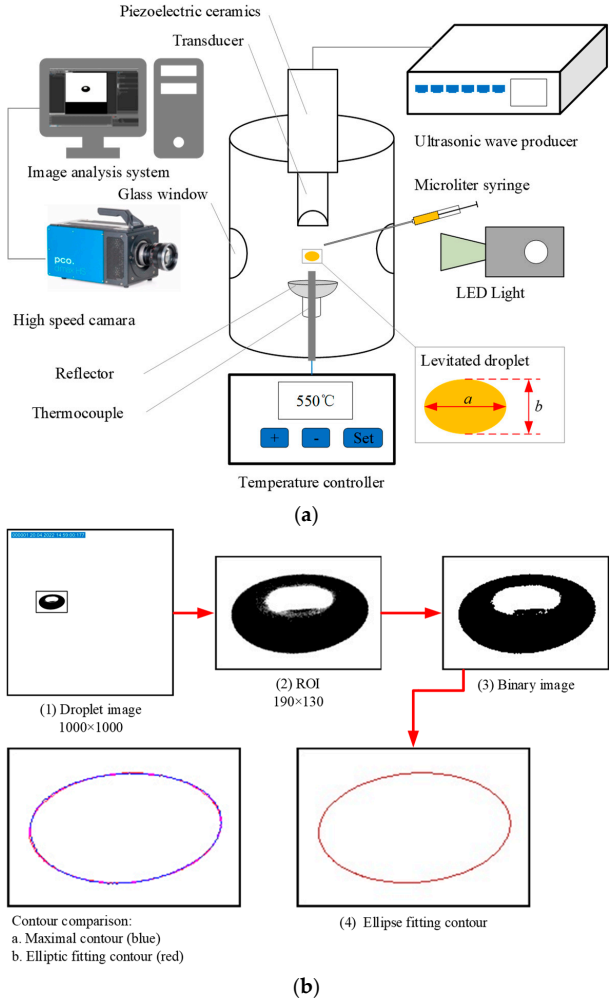

Figure 2. (**a**) The experimental setup for fuel droplet evaporation with acoustic levitation. (**b**) Droplet image processing process and contour comparison.

Hexadecane and diesel fuels with the parameters listed in Table 1 were used in our experiment. The temperature range of the investigation was 150~550 °C, with a measurement error range of ≤5 °C.

Table 1. Physical and chemical property parameters of fuels.

Item	Hexadecane	Diesel
Formula	$C_{16}H_{34}$	C_nH_{2n+2}
Average molecular weight	226	140~283
Boiling point (°C)	287	273~392
Density at 20 °C (g/cm^3)	0.77	0.81~0.85

Table 1. *Cont.*

Item	Hexadecane	Diesel
Latent heat of vaporization (KJ/ kg)	232	258
Kinematic viscosity at 20 °C (mm^2/s)	3.027	3.0~8.0
Saturated vapor pressure (MPa)	0.0995	-
Diffusion coefficient at 20 °C (m^2/s)	0.18×10^{-4}	-
Critical pressure (MPa)	1.44	1.90~2.20
Critical temperature (°C)	449	440~470

where $n \in [10, 22]$.

4. Results and Discussion

4.1. Fuel Droplet Evaporation Kinetics

Figure 3 illustrates the evaporation process of fuel droplets at different temperatures. The number located at the superior right-hand corner of every droplet corresponds to the evaporation time in seconds. Figure 4 shows the corresponding aspect ratio during their evaporation history.

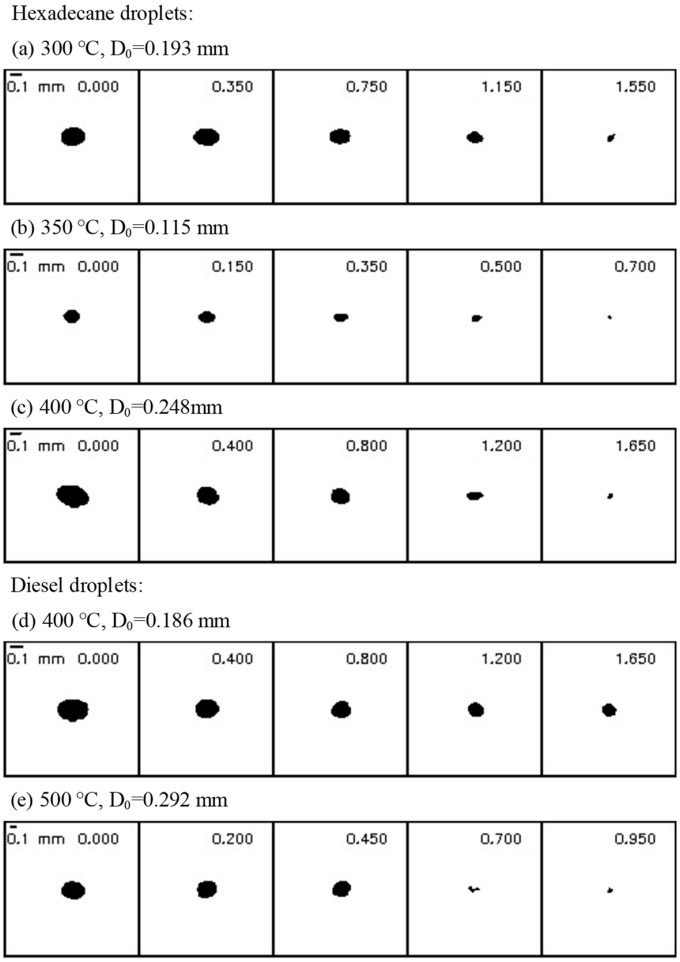

Figure 3. Levitated droplet evaporation at varied ambient temperatures. Hexadecane: (**a**–**c**) 300, 350, and 400 °C, with initial diameters of 0.193, 0.115, and 0.248 mm. Diesel: (**d**,**e**) temperatures are 400 and 500 °C.

The evaporation behaviors of acoustically suspended fuel droplets are visible (Figure 3). In Figure 4, the aspect ratio of the initial droplet ranges from 0.6 to 0.8 and changes with evaporation, indicating that the initial droplet is a flat sphere, and the droplet's shape also changes with evaporation. At 350 °C and 400 °C for hexadecane and 500 °C for diesel, the

final recorded aspect ratios reached one (Figure 3b,c,e). Evaporation leads to a decrease in the mass and an increase in the surface temperature of droplets [33]. Consequently, under acoustic radiation force and droplet gravity, droplets levitated in an acoustic field may have violent and disorderly fluctuations. In addition, the kinematic viscosity of droplets may also affect the oscillation [34,35]. Ultrasound waves exert control over the droplets; however, when the kinetic energy of the droplet reaches a certain threshold due to intensified oscillation, the droplet disengages from the acoustic field, causing it to descend. This complexity makes the experiments challenging, leading us to present only a subset of relatively reliable results for analysis.

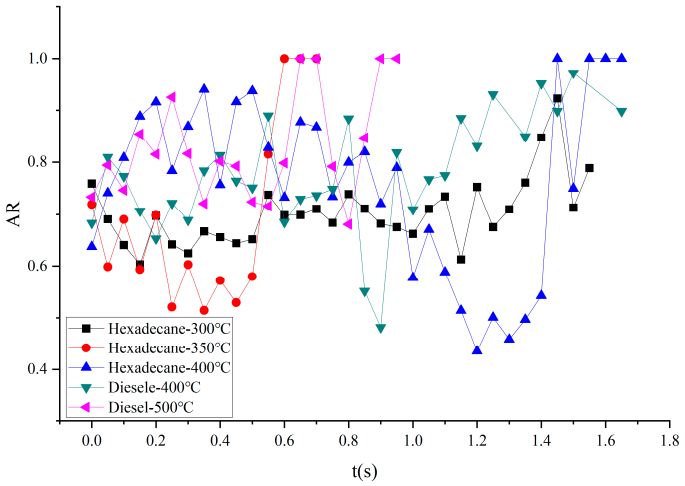

Figure 4. Aspect ratio of the acoustically levitated fuel droplet in Figure 3.

4.2. Effects of Temperature

Figure 5 depicts the impact of ambient temperature on the evaporation characteristics of acoustically levitated fuel droplets. The squares filled with different colors and connected by dotted lines represent the average evaporation rate of the droplets at various temperatures. The periodic oscillation of ultrasound waves [36] causes droplets to variously move with time in three-dimensional space, thus decreasing droplet surface area oscillations, as shown in Figure 5. Therefore, the mean evaporation rate at a constant state is chosen and computed as the evaporation rate (Equation (7)).

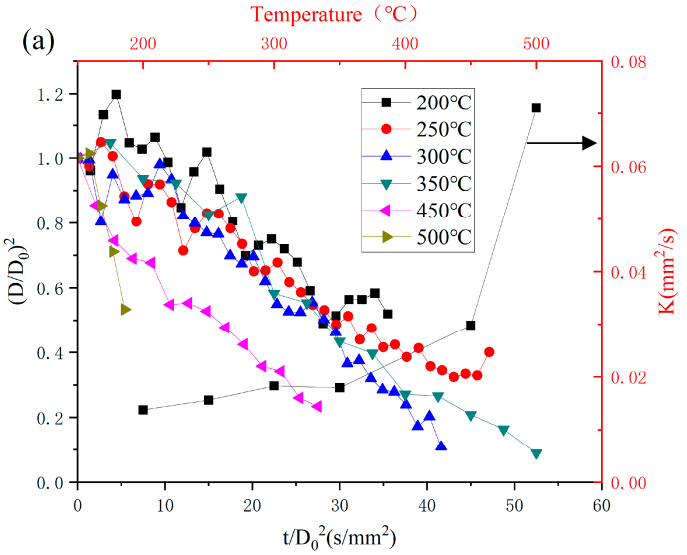

Figure 5. *Cont.*

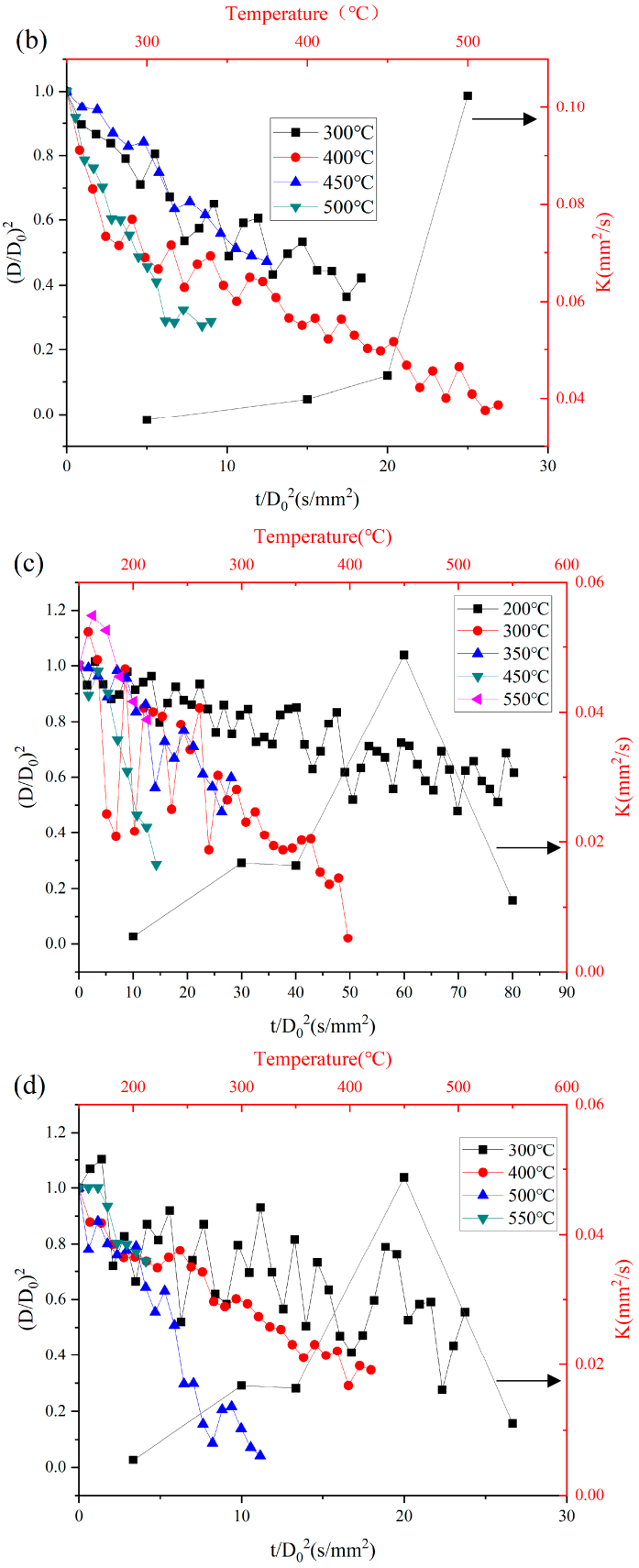

Figure 5. Effect of temperature on the evaporation characteristics of fuel droplets. Hexadecane droplet: (**a**) $D_0 \in (0.10, 0.20)$, temperature 200~550 °C, (**b**) $D_0 \in (0.20, 0.30)$, temperature 300~500 °C. Diesel droplet: (**c**) $D_0 \in (0.10, 0.20)$, temperature 200~550 °C, (**d**) $D_0 \in (0.20, 0.30)$, temperature 300~550 °C.

The evaporation rate rises dramatically when the ambient temperature reaches the critical temperature. Also, droplet expansion can be found at low temperatures. For hexadecane, the evaporation rate near the critical temperature is 60% greater than that under subcritical conditions when $D_0 \in (0.10, 0.20)$. But, when $D_0 \in (0.20, 0.30)$, it is only 26% greater than 300 °C and 12% greater than 400 °C. At 500 °C, both of the evaporation rates of the droplets with $D_0 \in (0.10, 0.20)$ and $D_0 \in (0.20, 0.30)$ are significantly faster than in subcritical conditions. High temperatures rapidly elevate the surface temperatures of droplets, effectively boosting heat transfer in their vicinity. Simultaneously, the increased saturated vapor pressure enhances mass transfer. The presence of an acoustic field capable of compressing the droplet and thereby expanding its surface area induces acoustic streaming near the droplet, potentially augmenting heat transfer and vapor diffusion. These dynamics highlight significant variations in evaporation rates at different temperatures. Hence, establishing a range of droplet diameters becomes a reasonable classification, thus enabling the analysis of the initial droplet diameter's impact on subsequent evaporation in the following section.

The droplet's surface area fluctuation is more evident for diesel droplets. The reason is that the kinematic viscosity decreases as droplet compositions evaporate. Also, the change in acoustic streaming structure may cause a non-linear shear change near the droplet surface [37] and increase the Reynolds number [38]. The evaporation of diesel droplets is like that of hexadecane droplets. The evaporation rate near critical temperatures is faster than in subcritical conditions. When $D_0 \in (0.10, 0.20)$, it is almost three times higher than 300 °C and 350 °C, and when $D_0 \in (0.20, 0.30)$, it is nearly 3.89 times higher than 300 °C and 2.25 times higher than 400 °C. The results show a difference from hexadecane.

The evaporation rates of hexadecane droplets with larger initial diameters show a minor increase as the surrounding gas temperature rises. In contrast, the evaporation rates of diesel droplets with larger initial diameters display relatively higher growth under identical conditions. This observation aligns with the characteristic easier-to-evaporate components in diesel droplets, indicating a prior evaporation behavior [6]. Figure 5c,d (Diesel droplets) show the temperature is up to 550 °C. However, the evaporation rate decreases. The diesel droplet is falling, and the evaporation is still not entering the steady stage. However, it is possible to observe that the lifespan of droplets may be considerably shorter in alternative scenarios.

4.3. Effects of Droplet Properties

4.3.1. Initial Diameters

The difference from the early experimental results in an acoustic field of fuel droplets [39,40] where $D_0 \in (0.98, 1.46)$ and $D_0 \in (1.30, 1.80)$ concludes that the evaporation rate is independent of the initial droplet diameter. Figure 6 shows that for both hexadecane and diesel droplets, the evaporation rate increases with the increase in the initial droplet diameter, where $D_0 \in (0.10, 0.30)$. Furthermore, our experimental results indicate that the influence of the initial droplet diameter on the evaporation rate becomes more pronounced with increasing temperature. This observation aligns with compressibility, heat transfer, and mass transfer theories regarding acoustically levitated droplets [38,41,42]. These theories suggest that a sizable initial droplet diameter corresponds to higher Sherwood and Nusselt numbers, leading to an accelerated heat and mass transfer rate. Also, other experiment results [16,43] show that a more significant initial diameter leads to a larger relative velocity and mass transfer rate.

4.3.2. Comparison of Different Fuels

Table 2 concisely compares the evaporation characteristics of diesel and hexadecane at comparable initial droplet diameters and temperatures. Meanwhile, Figure 7 illustrates the specific details of their respective evaporation behaviors.

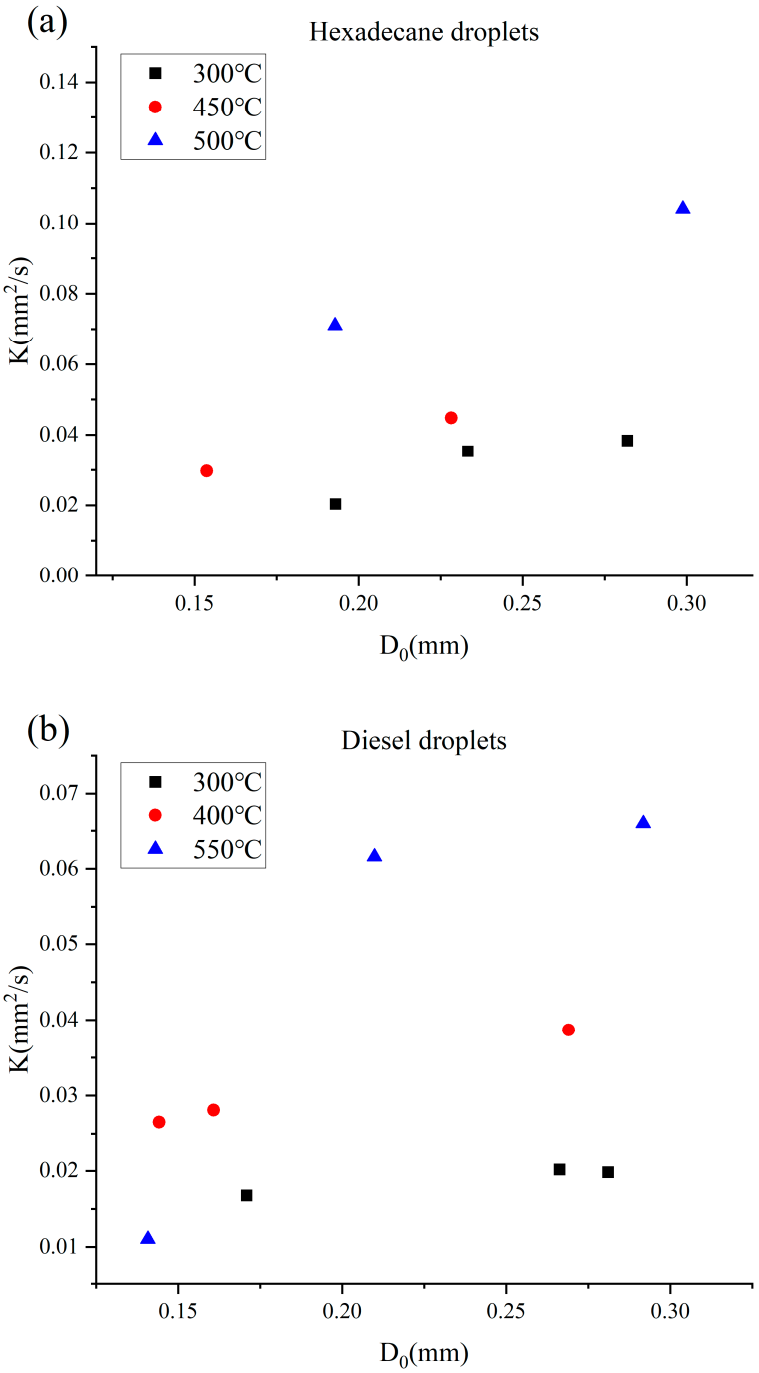

Figure 6. Influence of initial diameters on evaporation characteristics of fuel droplets. (**a**) Hexadecane, (**b**) diesel.

Table 2. Comparison of the evaporation of diesel and hexadecane under similar experimental conditions.

Temperature (°C)	Droplet	D_0(mm)	K(mm^2/s)
200	Hexadecane	0.183	0.01398
	Diesel	0.184	0.00562
300	Hexadecane	0.266	0.03837
	Diesel	0.282	0.02298
400	Hexadecane	0.269	0.04021
	Diesel	0.248	0.04099

Table 2. *Cont.*

Temperature (°C)	Droplet	D_0(mm)	K(mm^2/s)
450	Hexadecane	0.167	0.02980
	Diesel	0.154	0.04878
500	Hexadecane	0.292	0.10415
	Diesel	0.299	0.09074

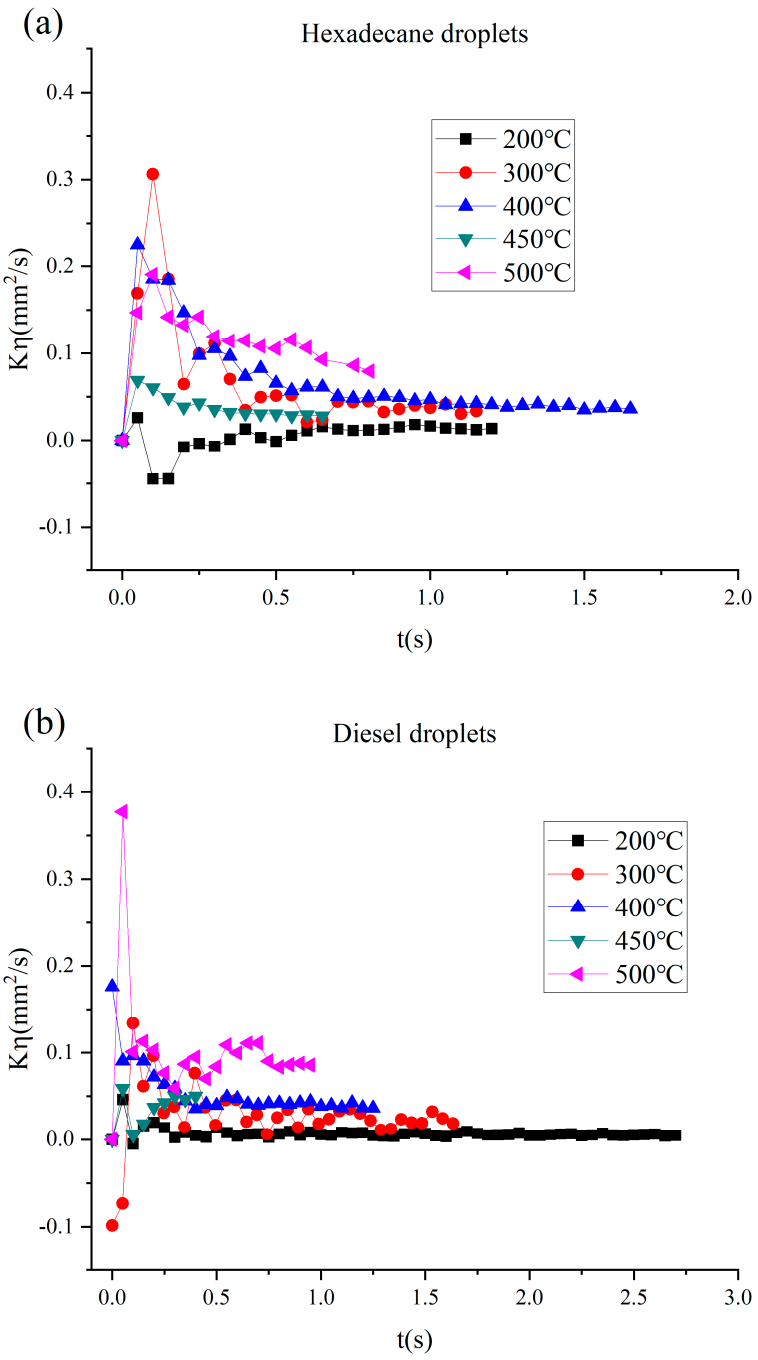

Figure 7. Effect of droplets' physical and chemical properties on evaporation characteristics of fuel droplets under similar initial diameters at 200 °C, 300 °C, 400 °C, 450 °C, and 500 °C. (**a**) Hexadecane, (**b**) Diesel.

Figure 7 shows that almost all of these fuel droplets have entered the steady-state evaporation stage and exhibit different behaviors. Except for 400 °C, the evaporation rates

for hexadecane and diesel are nearly identical. Hence, we conclude that at 400 °C, the component of cetane in diesel droplets is close to hexadecane. The distinction between the evaporation of the two fuel droplets can be seen when temperatures are 200 °C, 300 °C, 450 °C, and 500 °C. Therefore, we will analyze these differences next.

At 450 °C, the evaporation of diesel droplets is faster than that of hexadecane droplets. From Figure 7, it can be seen that the evaporation of diesel droplets has not entered a steady state, i.e., volatile components still control the evaporation behaviors. And, before entering steady-state evaporation, the diesel droplet escapes from the acoustic field. But, it does not influence the analysis of other cases.

Figure 7 also concludes that the evaporation of hexadecane droplets is faster than that of diesel droplets. At a lower temperature (200 °C), the evaporation rate of hexadecane is 2.49 times higher than that of diesel droplets. However, as gas temperatures rise to 300 °C and 500 °C, this ratio decreases to 1.71 and 1.45 times, respectively. This means that the diesel droplet has some non-volatile components [6].

5. Conclusions

Experimental investigation into the evaporation of acoustically levitated fuel droplets at high temperatures was conducted. Both hexadecane and diesel droplet evaporation have been conducted at temperatures between 150 and 550 °C, and the effects of temperature and droplet features on evaporation characteristics were examined. The results indicate that these fuel droplets have the potential to follow the D^2-law-governed steady-state evaporation stage.

The initial diameter of the droplet and the ambient temperature both directly affect the rate of evaporation. The equilibrium temperature of the droplet's surface increases with ambient temperature, and so does the evaporation rate. The initial droplet diameter significantly impacts the hexadecane or diesel droplet evaporation rate at lower compared to higher ambient temperatures.

At subcritical temperatures, the hexadecane droplet evaporates more quickly. Hexadecane droplets vaporize at a pace akin to diesel droplets when the environment is critical. Hexadecane vaporizes more rapidly than diesel droplets when the environment is supercritical. Hexadecane droplets may evaporate 15–71% more quickly than diesel droplets under similar initial droplet width and somewhat high ambient temperature.

In the future, acoustic levitation technology can be used to study fuel droplet evaporation under high-temperature and high-pressure conditions that are closer to the real conditions inside the cylinder of ICE. This would be of great importance to find ways to increase efficiency, optimize performance, and reduce emissions for the ICE industry.

Author Contributions: Conceptualization, B.P., X.L., W.L., Y.H. (Yongqing He), Z.Y. and T.D.; Methodology, Y.H. (Yongqing He), Z.S., Z.Y. and T.D.; Software, G.Y.; Formal analysis, G.Y.; Investigation, G.Y. and Y.H. (Yu Huang); Resources, G.Y. and Y.H. (Yu Huang); Data curation, G.Y. and Y.H. (Yu Huang); Writing—original draft, G.Y. and Y.H. (Yu Huang); Writing—review & editing, B.P., X.L., W.L., Y.H. (Yongqing He), Z.S., Z.Y. and T.D.; Visualization, G.Y. and Y.H. (Yu Huang); Supervision, Y.H. (Yongqing He), Z.Y. and T.D.; Project administration, B.P., X.L. and W.L.; Funding acquisition, Z.Y. All authors have read and agreed to the published version of the manuscript.

Funding: This work is supported by the Science Fund of the State Key Laboratory of Engine Reliability (No. skler-202015).

Data Availability Statement: Data are contained within the article.

Conflicts of Interest: Authors Bin Pang, Xiaoxin Liu and Wanli Li were employed by the Engine Research Institute, Weichai Power Co., Ltd. The remaining authors declare that the research was conducted in the absence of any commercial or financial relationships that could be construed as a potential conflict of interest.

References

1. Salama, R.S.; Mannaa, M.A.; Altass, H.M.; Ibrahim, A.A.; Khder, A.E.-R.S. Palladium supported on mixed-metal–organic framework (Co–Mn-MOF-74) for efficient catalytic oxidation of CO. *RSC Adv.* **2021**, *11*, 4318–4326. [CrossRef] [PubMed]
2. Broatch, A.; Carreres, M.; Garcia-Tiscar, J.; Belmar-Gil, M. Spectral analysis and modelling of the spray liquid injection in a Lean Direct Injection (LDI) gas turbine combustor through Eulerian-Lagrangian Large Eddy Simulations. *Aerosp. Sci. Technol.* **2021**, *118*, 106992. [CrossRef]
3. Lo Schiavo, E.; Laera, D.; Riber, E.; Gicquel, L.; Poinsot, T. On the impact of fuel injection angle in Euler-Lagrange large eddy simulations of swirling spray flames exhibiting thermoacoustic instabilities. *Combust. Flame* **2021**, *227*, 359–370. [CrossRef]
4. Mehrizi, A.A.; Karimi-maleh, H.; Naddafi, M.; Karaman, O.; Karimi, F.; Karaman, C.; Cheng, C.K. Evaporation characteristics of nanofuel droplets: A review. *Fuel* **2022**, *319*, 123731. [CrossRef]
5. Niimura, Y.; Hasegawa, K. Evaporation of droplet in mid-air: Pure and binary droplets in single-axis acoustic levitator. *PLoS ONE* **2019**, *14*, e0212074. [CrossRef] [PubMed]
6. Hinrichs, J.; Shastry, V.; Junk, M.; Hemberger, Y.; Pitsch, H. An experimental and computational study on multicomponent evaporation of diesel fuel droplets. *Fuel* **2020**, *275*, 117727. [CrossRef]
7. Jackson, D.P.; Chang, M.-H. Acoustic levitation and the acoustic radiation force. *Am. J. Phys.* **2021**, *89*, 383–392. [CrossRef]
8. Zang, D.; Tarafdar, S.; Tarasevich, Y.Y.; Dutta Choudhury, M.; Dutta, T. Evaporation of a Droplet: From physics to applications. *Phys. Rep.* **2019**, *804*, 1–56. [CrossRef]
9. Buchholz, M.; Haus, J.; Polt, F.; Pietsch, S.; Schönherr, M.; Kleine Jäger, F.; Heinrich, S. Dynamic model development based on experimental investigations of acoustically levitated suspension droplets. *Int. J. Heat Mass Transf.* **2021**, *171*, 121057. [CrossRef]
10. Polachini, T.C.; Mulet, A.; Telis-Romero, J.; Cárcel, J.A. Acoustic fields of acid suspensions containing cassava bagasse: Influence of physical properties on acoustic attenuation. *Appl. Acoust.* **2021**, *177*, 107922. [CrossRef]
11. Pandiselvam, R.; Aydar, A.Y.; Kutlu, N.; Aslam, R.; Sahni, P.; Mitharwal, S.; Gavahian, M.; Kumar, M.; Raposo, A.; Yoo, S.; et al. Individual and interactive effect of ultrasound pre-treatment on drying kinetics and biochemical qualities of food: A critical review. *Ultrason. Sonochem.* **2023**, *92*, 106261. [CrossRef] [PubMed]
12. Al Zaitone, B. Evaporation of oblate spheroidal droplets: A theoretical analysis. *Chem. Eng. Commun.* **2018**, *205*, 110–121. [CrossRef]
13. Prud'homme, R.; Habiballah, M.; Matuszewski, L.; Mauriot, Y.; Nicole, A. Theoretical Analysis of Dynamic Response of a Vaporizing Droplet to Acoustic Oscillations. *J. Propuls. Power* **2010**, *26*, 74–83. [CrossRef]
14. Combe, N.A.; Donaldson, D.J. Water Evaporation from Acoustically Levitated Aqueous Solution Droplets. *J. Phys. Chem. A* **2017**, *121*, 7197–7204. [CrossRef] [PubMed]
15. Sasaki, Y.; Hasegawa, K.; Kaneko, A.; Abe, Y. Heat and mass transfer characteristics of binary droplets in acoustic levitation. *Phys. Fluids* **2020**, *32*, 072102. [CrossRef]
16. Meshkinzar, A.; Al-Jumaily, A.M. Acoustically enhanced evaporation of a polydisperse stream of micro water droplets. *J. Aerosol. Sci.* **2020**, *139*, 105466. [CrossRef]
17. Berdugo, N.; Stolar, M.; Liberzon, D. Enhancement of water droplet evaporation rate by application of low frequency acoustic field. *Int. J. Multiph. Flow* **2020**, *126*, 103217. [CrossRef]
18. Fumachi, E.F.; Toledo, R.C.; Tenório, P.I.G.; An, C.Y.; Bandeira, I.N. Heat Transfer in the Samples Solidified in Drop Tubes. *Microgravity Sci. Technol.* **2019**, *31*, 185–194. [CrossRef]
19. Zhang, P.; Chen, C.; Guo, F.; Philippe, J.; Gu, Y.; Tian, Z.; Bachman, H.; Ren, L.; Yang, S.; Zhong, Z.; et al. Contactless, programmable acoustofluidic manipulation of objects on water. *Lab A Chip* **2019**, *19*, 3397–3404. [CrossRef]
20. Ali Al Zaitone, B.; Tropea, C. Evaporation of pure liquid droplets: Comparison of droplet evaporation in an acoustic field versus glass-filament. *Chem. Eng. Sci.* **2011**, *66*, 3914–3921. [CrossRef]
21. Yarin, A.L.; Brenn, G.; Rensink, D. Evaporation of acoustically levitated droplets of binary liquid mixtures. *Int. J. Heat Fluid Flow* **2002**, *23*, 471–486. [CrossRef]
22. Schiffter, H.; Lee, G. Single-Droplet Evaporation Kinetics and Particle Formation in an Acoustic Levitator. Part 2: Drying Kinetics and Particle Formation from Microdroplets of Aqueous Mannitol, Trehalose, or Catalase. *J. Pharm. Sci.* **2007**, *96*, 2284–2295. [CrossRef] [PubMed]
23. Brenn, G.; Deviprasath, L.J.; Durst, F.; Fink, C. Evaporation of acoustically levitated multi-component liquid droplets. *Int. J. Heat Mass Transf.* **2007**, *50*, 5073–5086. [CrossRef]
24. Sharma, S.; Jain, S.; Saha, A.; Basu, S. Evaporation dynamics of a surrogate respiratory droplet in a vortical environment. *J. Colloid Interface Sci.* **2022**, *623*, 541–551. [CrossRef] [PubMed]
25. Andrade, M.A.B.; Pérez, N.; Adamowski, J.C. Review of Progress in Acoustic Levitation. *Braz. J. Phys.* **2018**, *48*, 190–213. [CrossRef]
26. Moslabeh, F.G.Z.; Fouladgar, F.; Jafari, A.; Habibi, N. Substrate-free self-assembly of peptides nano-particles through acoustic levitation. *Colloids Surf. A Physicochem. Eng. Asp.* **2023**, *657*, 130439. [CrossRef]
27. Basu, S.; Saha, A.; Kumar, R. Criteria for thermally induced atomization and catastrophic breakup of acoustically levitated droplet. *Int. J. Heat Mass Transf.* **2013**, *59*, 316–327. [CrossRef]

28. Li, Z.; Yang, G.; Peng, Z.; Liu, X.; Hu, X.; Yu, H.; Liu, J.; Liu, W.; Shi, Z.; He, Y.; et al. Experimental investigation on evaporation of a single droplet levitated in acoustic field. In Proceedings of the 2022 20th International Conference on Mechatronics—Mechatronika (ME), Pilsen, Czech Republic, 7–9 December 2022; pp. 1–5. [CrossRef]
29. Argyri, S.-M.; Evenäs, L.; Bordes, R. Contact-free measurement of surface tension on single droplet using machine learning and acoustic levitation. *J. Colloid Interface Sci.* **2023**, *640*, 637–646. [CrossRef]
30. Al Zaitone, B. Oblate spheroidal droplet evaporation in an acoustic levitator. *Int. J. Heat Mass Transf.* **2018**, *126*, 164–172. [CrossRef]
31. Leiterer, J.; Delissen, F.; Emmerling, F.; Thünemann, A.F.; Panne, U. Structure analysis using acoustically levitated droplets. *Anal. Bioanal. Chem.* **2008**, *391*, 1221–1228. [CrossRef]
32. Prasad, S.; Narayanan, S.; Mandal, D.K. Acoustic induced flow around an evaporating drop and its influence on internal circulation. *Int. J. Multiph. Flow* **2019**, *116*, 91–99. [CrossRef]
33. Bänsch, E.; Götz, M. Numerical study of droplet evaporation in an acoustic levitator. *Phys. Fluids* **2018**, *30*, 037103. [CrossRef]
34. Yarin, A.L.; Weiss, D.A.; Brenn, G.; Rensink, D. Acoustically levitated drops: Drop oscillation and break-up driven by ultrasound modulation. *Int. J. Multiph. Flow* **2002**, *28*, 887–910. [CrossRef]
35. Hasegawa, K.; Watanabe, A.; Kaneko, A.; Abe, Y. Internal flow during mixing induced in acoustically levitated droplets by mode oscillations. *Phys. Fluids* **2019**, *31*, 112101. [CrossRef]
36. Liu, L.-H.; Han, Y.-F.; Wang, Q.; Fu, Q.-F. Molecular dynamics simulation of droplet evaporation in a one-dimensional standing wave acoustic field. *Int. J. Therm. Sci.* **2023**, *184*, 107939. [CrossRef]
37. Kobayashi, K.; Goda, A.; Hasegawa, K.; Abe, Y. Flow structure and evaporation behavior of an acoustically levitated droplet. *Phys. Fluids* **2018**, *30*, 5037728. [CrossRef]
38. Shitanishi, K.; Hasegawa, K.; Kaneko, A.; Abe, Y. Study on Heat Transfer and Flow Characteristic Under Phase-Change Process of an Acoustically Levitated Droplet. *Microgravity Sci. Technol.* **2014**, *26*, 305–312. [CrossRef]
39. Saito, M.; Sato, M.; Suzuki, I. Evaporation and combustion of a single fuel droplet in acoustic fields. *Fuel* **1994**, *73*, 349–353. [CrossRef]
40. Saito, M.; Hoshikawa, M.; Sato, M. Enhancement of evaporation/combustion rate coefficient of a single fuel droplet by acoustic oscillation. *Fuel* **1996**, *75*, 669–674. [CrossRef]
41. Yarin, A.L.; Brenn, G.; Kastner, O.; Rensink, D.; Tropea, C. Evaporation of acoustically levitated droplets. *J. Fluid Mech.* **1999**, *399*, 151–204. [CrossRef]
42. Wulsten, E.; Lee, G. Surface temperature of acoustically levitated water microdroplets measured using infra-red thermography. *Chem. Eng. Sci.* **2008**, *63*, 5420–5424. [CrossRef]
43. Mondragon, R.; Hernandez, L.; Enrique Julia, J.; Carlos Jarque, J.; Chiva, S.; Zaitone, B.; Tropea, C. Study of the drying behavior of high load multiphase droplets in an acoustic levitator at high temperature conditions. *Chem. Eng. Sci.* **2011**, *66*, 2734–2744. [CrossRef]